

# Transformer-based Multimodal Change Detection with Multitask Consistency Constraints

Biyuan Liu<sup>a</sup>, Huaixin Chen<sup>a</sup>, Kun Li<sup>b</sup>, Michael Ying Yang<sup>b</sup>

<sup>a</sup>*School of Resources and Environment, University of Electronic Science and Technology of China, Chengdu, 611731, Sichuan, China*

<sup>b</sup>*Faculty of GeoInformation Science and Earth Observation (ITC), University of Twente, Drienerlolaan 5, Enschede, 7522 NB, The Netherlands*

---

## Abstract

Change detection plays a fundamental role in Earth observation for analyzing temporal iterations over time. However, recent studies have largely neglected the utilization of multimodal data that presents significant practical and technical advantages compared to single-modal approaches. This research focuses on leveraging digital surface model (DSM) data and aerial images captured at different times for detecting change beyond 2D. We observe that the current change detection methods struggle with the multitask conflicts between semantic and height change detection tasks. To address this challenge, we propose an efficient Transformer-based network that learns shared representation between cross-dimensional inputs through cross-attention. It adopts a consistency constraint to establish the multimodal relationship, which involves obtaining pseudo change through height change thresholding and minimizing the difference between semantic and pseudo change within their overlapping regions. A DSM-to-image multimodal dataset encompassing three cities in the Netherlands was constructed. It lays a new foundation for beyond-2D change detection from cross-dimensional

inputs. Compared to five state-of-the-art change detection methods, our model demonstrates consistent multitask superiority in terms of semantic and height change detection. Furthermore, the consistency strategy can be seamlessly adapted to the other methods, yielding promising improvements.

*Keywords:*

change detection, multimodal, height change, multitask consistency, Transformer-based

---

## 1. Introduction

The field of change detection is undergoing a significant evolution characterized by higher temporal frequencies, finer-grained analyses, and increased dimensionality. Recent advancements in Earth observation techniques have enabled daily change detection [1] and fine-grained analysis spanning up to nine distinct change categories [2]. Moreover, there have been exciting breakthroughs beyond traditional 2D change detection [3, 4]. However, a predominant number of prevailing developments still center around single-modal and 2D change detection, such as introducing contrastive metrics for learning class-distinct features [5, 6], leveraging multitask consistency for semi-supervised training [7, 8] and adopting attention mechanisms to model long-range context [9, 10].

Some noteworthy examples have demonstrated the incorporation of multimodal data into change detection task offers both practical flexibility and technical advantages. Combining optical images with synthetic aperture radar (SAR) [11, 12] can alleviate weather-related and atmospheric restrictions. Using point cloud data from Lidar and photogrammetry [13] for de-

tecting 3D changes is obviously less constrained in input pairs formation, resulting in enhanced flexible application. Furthermore, the different imaging modalities may be complementary for enhancing the change detection in some extreme conditions (e.g. flooding [14] and burned areas [15]). In our specific scenario, the integration of DSM and aerial imagery introduces crucial vertical information, facilitating change detection at a finer scale and extending beyond traditional 2D semantic change detection.

Due to the scarcity of bi-temporal 3D data, existing methods for high dimensional change detection often utilize multi-source 3D data that require manual modality alignment before change detection, such as dense image matching [16] and artificial feature selection [13, 17], which are time-consuming processes that risk information loss. In MTBIT [18], bi-temporal 2D images are employed to infer building height change, inadvertently neglecting the advantages of multimodal data, as exhaustively noted in section 2. Consequently, there remains a lack of exploration of change detection beyond 2D that fully leverages the potential of multimodal data.

To bridge these gaps and confront the inherent challenges, we first construct a multi-temporal dataset named Hi-BCD, which involves DSM (Height data) and aerial image pairs for detecting multi-category semantic and height building changes, encompassing three cities in the Netherlands. Through extensive benchmarking of five state-of-the-art methods, including convolutional neural network (CNN) based and Transformer-based methods, we discover the potential multitask conflicts between semantic change detection (classification task) and height change detection (regression task). As shown in Figure 1, the multitask branches have brought great impact on each

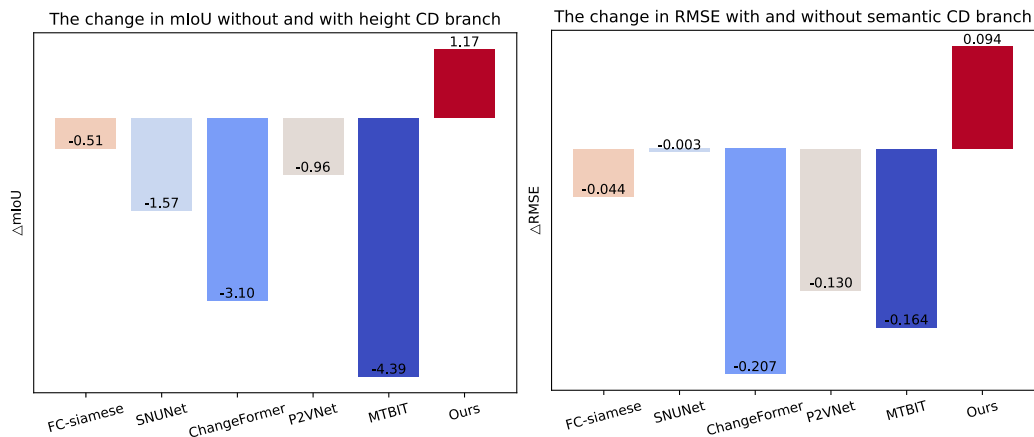


Figure 1: The performance change of semantic (left) and height (right) change detection in single-task and multitask manner, which implies the multitask conflicts between 2D semantic and height change detection.

other. The performance of semantic change detection branch declined due to the height branch, while the height change detection branch conversely gained some improvements due to semantic hints. Therefore, we propose a novel Transformer-based pipeline that learns shared representation from images and DSM data via cross-attention. It is equipped with an explicit multitask consistency strategy, which involves the mapping from continuous height change to semantic-aware pseudo change with soft-thresholding module. Then the pixel-wise similarity is maximized between pseudo change and real semantic change, enabling the information interaction of multimodal change maps. The contributions of this paper are summarized as follows:

- We propose an efficient and light Transformer-based network that handles the feature fusion of cross-dimensional modalities via parallelly arrange cross-attention modules.

- We reveal the potential multitask conflicts in state-of-the-art methods while simultaneously handling semantic and height change detection. We propose a multitask consistency constraint that quantifies the similarity between semantic and pseudo change obtained through height change thresholding for alleviating multitask interference.
- We build a multimodal DSM-to-image dataset with generously sized high-resolution tiles, which enables the detection of 2D semantic and 3D height changes simultaneously from cross-dimensional modalities. The experiment demonstrates that our method outperforms existing methods with consistent semantic and height change detection results. Additionally, the consistency strategy can be easily employed to enhance the other methods.

The rest of this paper is organized as follows: Section 2 provides a brief overview of single-modal and multimodal change detection methods. Section 3 introduces the proposed multimodal change detection network and multitask consistency. Section 4 describes our dataset. In Section 5, we perform a comparison with some current state-of-the-art convolutional neural network (CNN) based and Transformer-based change detection models, which reveals the multitask conflicts and demonstrates the superiority of our method. We conduct ablation studies about the influence of multitask consistency in semantic and height change detection, providing a better understanding of our model. Section 6 draws conclusions.

## 2. Related Work

**Single-modal change detection.** The most remarkable achievements occur in the field of single-modal 2D image change detection, where large-scale data are available for utilization. These studies have improved the accuracy and efficiency with superior training metrics [5, 6], densely-connected structure [19, 20], enhanced local and global context aggregation [21, 9], light-weight components [22] and decoupled change modeling [23]. Some latest studies also focus on detecting multi-class semantic changes for in-depth scene understanding [24, 2].

It is a significant trend that also challenges to detect the volumetric or vertical information in real applications such as quantitative estimation of changes in urban areas, forest biomasses, and land morphology [25, 18]. As multi-view imaging and aerial laser scanning (ALS) technologies continue to advance, an increasing amount of DSM-to-DSM [3] and cloud-to-cloud differencing methods [25, 26] have emerged. However, it is actually a strong hypothesis that the multi-temporal data are available, especially for 3D data, leaving a barrier to the wide applicability of these methods.

**Multimodal change detection.** A large number of multimodal change detection studies focus on detecting changes between optical and SAR images to alleviate the restriction of weather and atmosphere. Due to the scarcity of multimodal data, they tend to build the pixel-wise or graph correlation in an unsupervised manner without considering the deep features, such as the energy-based model [11], coupled dictionary learning [27], Markov random field model [14], change vector analysis [28], and graph representation learning [12, 29]. As for these deep learning methods, the majority employ an

explicit image translation process [30, 31, 32], while others opt for a single-modal change detection backbone to project two heterogeneous images into a shared latent space [33, 34].

Some recent efforts are delving into change detection beyond 2D with multimodal data. In [35], the Siamese CNN was employed to detect changes between point clouds obtained from ALS and dense image matching. In [17], the features including color, shape, and elevation maps are manually extracted for change detection between the point cloud and image. In [16], a multi-source point cloud processing network was devised to detect genuine 3D changes. Yet, most of these methods require a time-consuming pre-processing step for modality alignment, which potentially results in information loss. Conversely, we directly handle multimodal data across different dimensions inspired by cross-attention mechanisms [36].

In MTBIT [18], it attempted to infer a change map represented by DSM from bi-temporal 2D images. Unlike MTBIT, we propose to directly deal with DSM-to-image multimodal inputs for various reasons: 1) Estimating height from single view image remains an ill-posed problem. The introduced pre-temporal DSM provides abundant context priors about vertical information near the change areas. 2) The ground truth elevation change is essentially generated with bi-temporal DSMs, either in MTBIT or our method. Therefore, it is under-utilization of a considerable amount of 3D information in MTBIT. 3) For change detection that spans over a long time, there may exist a significant resolution gap in multi-temporal images (e.g., 2.0m vs. 0.25m as shown in Figure 6(a)(c)). On the contrary, the DSM data derived from point cloud in our dataset allows for at least 4 point records at a

$0.25 \times 0.25 m^2$  grid.

**Multitask learning in change detection.** It’s a natural intuition to introduce multitask constraints in change detection task. The typical idea is to predict the segmentation boundaries of bi-temporal inputs [37, 38, 39], where the learned representation can be shared with the change detection branch. The auxiliary constraint is usually beneficial, as it introduces inductive bias through the inclusion of related additional information. Nonetheless, as reported in [40], it can sometimes hamper the performance of each individual task. Certain studies have delved into the multitask relationship by considering multitask consistency. In [2], three consistency metrics including binary, change area, and no-change area consistency are used for evaluation. In [41], the consistency between bi-temporal semantic labels and the change labels is exploit to enhance semi-supervised generalization.

In our specific context, we address the issue of multitask conflicts within current change detection methods by focusing on the coherence between semantic and height variations. We highlight the connection between negatively changed height, often associated with demolished buildings, and positively changed height, as observed in newly constructed areas.

### 3. Method

#### *3.1. MMCD: Transformer-based multimodal change detection network*

**Efficient Pyramid backbone.** We pursuit an efficient and light-weight backbone architecture as the data volume in remote sensing is always large. For the backbone, we adopt the efficient Transformer block with sequence reduction as [42, 43]. Moreover, we reduce the embedding dimensions to



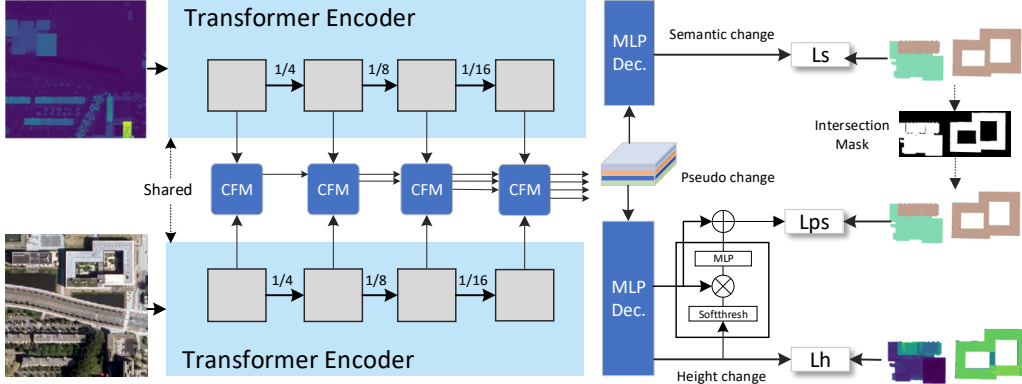


Figure 2: Our Transformer-based multimodal change detection pipeline is named MMCD. It consists of the pyramid backbone with four Transformer layers, the cross-modal fusion module (CFM), and multi-layer perception (MLP) decoder. The multitask consistency acts as an explicit constraint for enhancing multimodal correlation.

obtain a smaller model size with only half the complexity of ChangeFormer [43]. The pyramid feature outputs of height and image branch are  $X_H^n$  and  $X_I^n$ , where  $n \in \{1, 2, 3, 4\}$ .

**Cross-modal fusion.** To bridge the modality gap between height data and image data and learn discriminative shared representations, we draw the inspiration of cross-attention [36] and design the cross-modal fusion module as shown in Figure 3(a). It parallelly takes the feature embedding from one modality as query, and the embedding from the other modality as key and value. The standard self-attention component is

$$\text{attention}(X) = \text{softmax}(QK)V = \text{softmax}\left(\left(W_q X\right)\left(W_k X\right)^T\right)W_v X, \quad (1)$$

where  $W_q, W_k$  and  $W_v \in R^{C \times d}$  are learnable matrices,  $X \in \mathbb{R}^{d \times C}$  is input sequence, and the softmax is  $e^{x_i} / \sum_{j=1}^N e^{x_j}$ . The  $C$  is sequence length and  $d$  is embedding dimension. The left cross-attention block in Figure 3(a) can be

formulated as

$$\text{cross-attention}(X_H^n, X_I^n) = \text{softmax} \left( (W_q X_H^n)(W_k X_I^n)^T \right) W_v X_I^n. \quad (2)$$

The CFM uses two symmetrically arranged cross-attention operators for capturing mutual relationship between features derived from the DSM and image branches. Next, they are merged through MLP and convolutional unit, which is then pixel-wise added to the previous feature layer  $f^{n-1}$  to obtain  $f^n$ .

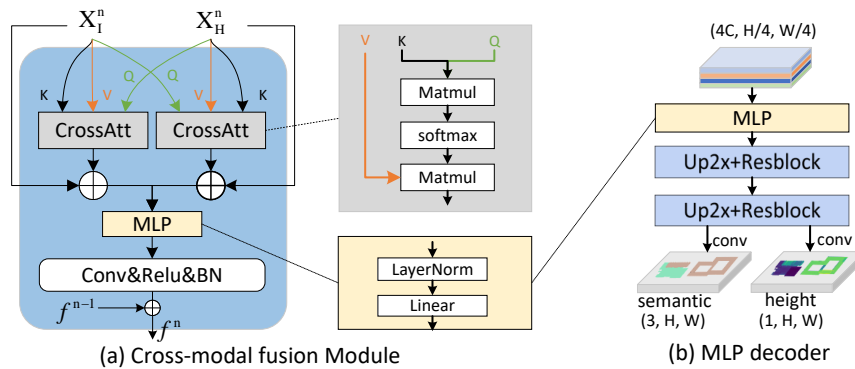


Figure 3: The structure of feature fusion module and decoder in our method.

**MLP decoder.** Figure 3(b) depicts the simple structure of our MLP decoder. We use non-parameterized up-sampling, while ChangeFormer[43] utilizes learnable transposed-convolution that incurs higher computation cost. Furthermore, the residual convolutional blocks [44] are utilized to enhance the local relations while up-sampling. The final semantic and height change map are obtained through  $3 \times 3$  convolution block as MTBIT [18].

### 3.2. Multitask consistency by predicting the pseudo semantic change

We correlate the height change detection task to the semantic change detection task with an explicit consistency constraint through predicting the

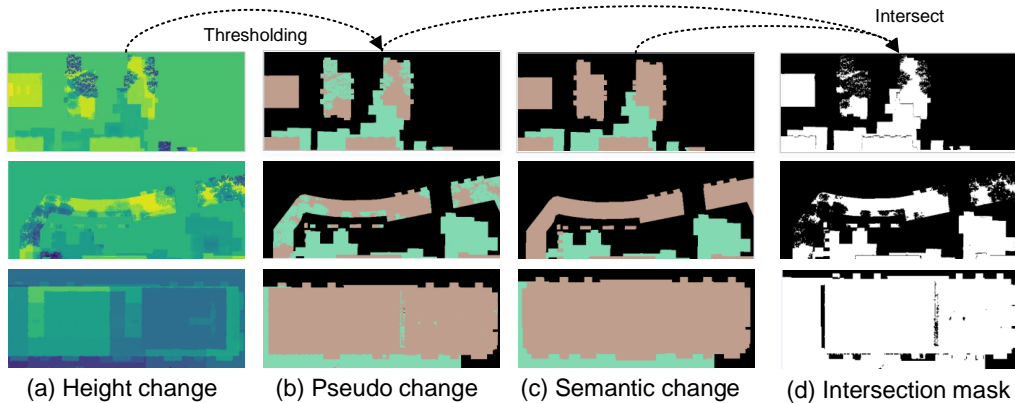


Figure 4: The inconsistency of multimodal change labels. (a) height change; (b) pseudo change by classifying the zero height as unchanged, positive height as newly-built and negative height as demolished regions; (c) semantic change; (d) intersection mask between height change and pseudo change, where the intersection rate of training, validation, and testing set are 79.71%, 89.23% and 90.03% respectively.

auxiliary pseudo-change map. There exists a gap between the semantic and height change, as the former are integral category values, while the latter are continuous floating values, corresponding to classification and regression tasks. As shown in Figure 4(a)(b), by adopting the zero as threshold on the height change, we obtain a classification map termed pseudo change that includes three classes: 0 (the background), 1 (positive) and the -1 (negative) height change, which differs from the semantic change (Figure 4(c)). The hard thresholding can be formulated as

$$T_h(x) = \begin{cases} 1, & x > 0 \\ 0, & x = 0 \\ -1, & x < 0. \end{cases} \quad (3)$$

Since it is not differential, we adopt a soft thresholding function as follow

$$T_s(x) = 2 \times \text{sigmoid}\left(\frac{x}{t}\right) - 1, \quad (4)$$

where  $\text{sigmoid} = 1/(1 + e^{-x})$ , and  $t$  is a positive temperature parameter for controlling the sharpness of the transition around zero. In our experiment, we set  $t = 0.5$ . Smaller  $t$  leads to a more accurate approximation to  $T_h(x)$ . In practice, this can be implemented with a sigmoid and a MLP layer for introducing strong prior to the pseudo change branch. The pseudo change highly overlaps with semantic change but not totally the same as shown in Figure 4(d). Therefore, only overlapped areas are considered when measuring the consistency between them, which is to minimize the following objective function

$$\mathcal{L}_{\text{consistency}} = \min_{\text{Pred}_{sc}, \text{Pred}_{psc}} (GT_{psc} \cap GT_{sc}) * |\text{Pred}_{psc} - \text{Pred}_{sc}|, \quad (5)$$

where  $|\cdot|$  is kind of distance.  $GT_{sc}$  and  $GT_{psc}$  are ground truth of semantic and pseudo change.  $\text{Pred}_{sc}$  and  $\text{Pred}_{psc}$  are corresponding model prediction. In practical implementation, the semantic and pseudo change branches are separately supervised with  $GT_{sc}$  and  $GT_{psc}$  respectively, which leads to consistency in their overlapping regions.

### 3.3. Loss function

We employ the weighted cross-entropy loss for both the semantic and pseudo change detection branches, and utilize mean-square error for the height change detection branch as [18], which are denoted as  $\mathcal{L}_{\text{height}}$ ,  $\mathcal{L}_{\text{pseudo}}$ , and  $\mathcal{L}_{\text{semantic}}$  respectively. The final training loss is

$$\mathcal{L}_{\text{total}} = \lambda_1 \cdot \mathcal{L}_{\text{pseudo}} + \lambda_2 \cdot \mathcal{L}_{\text{height}} + \lambda_3 \cdot \mathcal{L}_{\text{semantic}} \quad (6)$$

where  $\lambda_1$ ,  $\lambda_2$ , and  $\lambda_3$  are fixed loss weights, which are 0.2, 0.2, and 0.6 in our experiment setting.

#### 4. Hi-BCD: A multimodal dataset for building change detection between height map and optical image

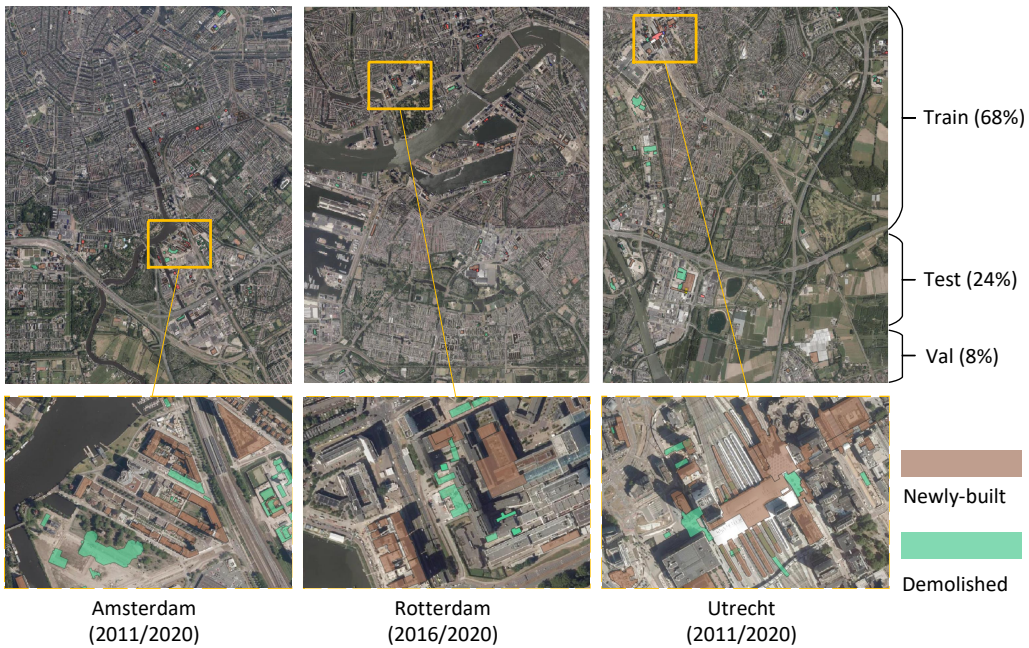


Figure 5: Hi-BCD dataset. It encompasses three cities in the Netherlands and provides two types of building changes. The dates of early and late periods are denoted under each city. For each city, 68%, 24%, and 8% of the tile are used for training, testing, and validation, respectively.

**Existing datasets and limitations.** Table 1 presents a concise comparison of existing change detection datasets, encompassing both single-modal and multimodal datasets. There is a substantial volume of bi-temporal 2D image datasets available, supporting high-resolution, high-frequency, and

multi-class change analysis. Despite the abundance of single-modal datasets, limited research has ventured beyond 2D change detection using multimodal data. The **Shuguang** dataset used in [12] contains a pair of SAR and optical image for detecting 2D construction change. The constraint of a small sample size dictates that the majority of methods can only be developed from an unsupervised standpoint. For **multimodalCD** [13], it incorporates multi-view image-based and ALS-based point clouds, which are transformed into DSMs to detect binary 2D changes exclusively. However, it confines its focus to 2D changes within small tile sizes, even though it contains beyond-2D information. For **3DCD** [18], it employs bi-temporal images to identify not only binary building changes but also variations in height. However, the resolution of height change is merely half that of 2D changes, and it exclusively classifies binary changes. To establish a new foundation for change detection that leverages multimodal inputs and simultaneously outputs semantic and height changes, we create the Hi-BCD dataset, which provides generously sized tiles and offers both high-resolution 2D and 3D semantic change maps.

Table 1: The main details of typical existing change detection datasets.

Name	N. images	Tile size	Resolution	CD map	Classes
LEVIR-CD [45]	637	1024 × 1024	0.5 m	2D	2
Hi-UCD [2]	40800	512 × 512	0.1 m	2D	9
DynamicEarthNet [1]	54750	1024 × 1024	3 m	2D	7
Shuguang [12]	1	921 × 593	-	2D	1
multimodalCD [13]	3615	100 × 100	0.1 m	2D	2
3DCD [18]	472	400 × 400	0.5 / 1m	2D / 3D	1
Hi-BCD (ours)	1500	1000 × 1000	0.25 m	2D / 3D	2

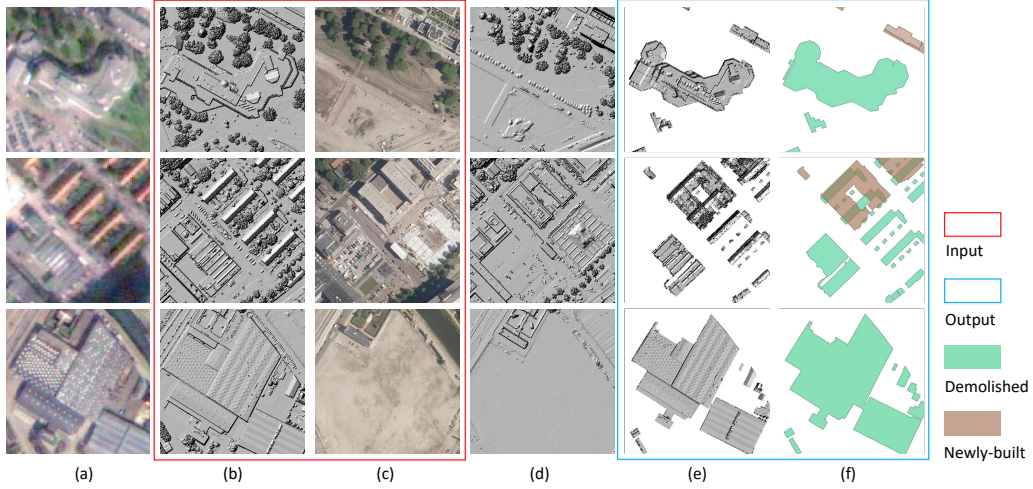


Figure 6: Examples of Hi-BCD dataset, where the DSMs are displayed in hillshade manner (A widely used visual technique to give a three-dimensional appearance from DSM data). The (a) and (b) are pre-temporal images (**2.0m** resolution) and DSMs (**0.25m** resolution). The (c) and (d) are post-temporal images and DSMs (all **0.25m** resolution). The (e) and (f) are height and semantic changes between the multimodal temporal inputs.

**Dataset overview.** As shown in Figure 5, our study area involves three cities in the Netherlands, including Amsterdam, Rotterdam, and Utrecht. The dates of the pre-temporal and post-temporal periods are indicated beneath each city in Figure 5. We can observe significant variation in the capture dates of the pre-temporal DSM, which reflects the extensive updating period of high-dimensional data. This hinders the application of high-dimensional change detection with dual-temporal 3D data. The data volume of a city consists of five hundreds of  $1000 \times 1000$  DSM-to-image pairs with a ground sampling distance of 0.25 meter (Figure 6(b)(c)) and the corresponding multi-class 3D and 2D changes (Figure 6(e)(f)). The vertical accuracy is about 0.15 meter [3]. For each city tile, 68%, 24%, and 8% are allocated for

Table 2: The main details of the Hi-BCD dataset, including changed objects, pixels, and sample amount of three cities in the Netherlands.

Attribute	Category	Amsterdam	Rotterdam	Utrecht
changed objects	newly-built	389	510	458
	demolished	251	229	187
changed pixels	amount	6.625M	5.139M	7.73M
	<i>prop/total</i>	1.3%	1.0%	1.5%
samples (size: $1k \times 1k$ )	total	500	500	500
	with change	40.8%	34.2%	43%

training, testing, and validation respectively. Two types of change including 'newly-built' and 'demolished' are defined in the dataset. More details about change objects, pixels, and samples are provided in Table 2. Figure 7 portrays the cumulative frequency of height for the two types of change.

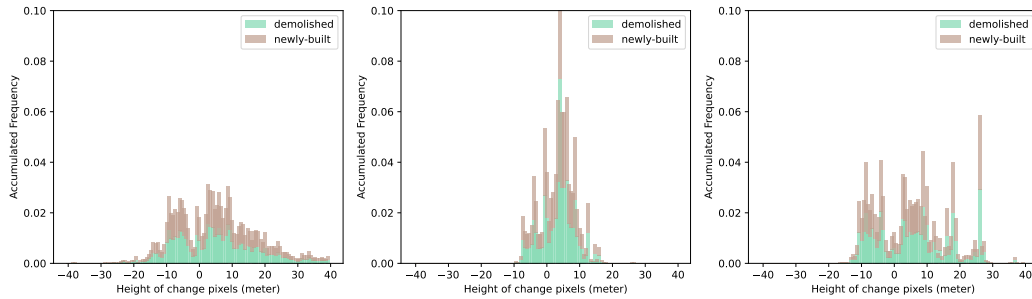


Figure 7: The cumulative frequency of height values for two types of change pixels.

**Annotation procedure.** We build the dataset based on AHN<sup>1</sup> (Actueel Hoogtebestand Nederland), the nationwide elevation data project in the Netherlands. To be specifically, the early-period elevation data are obtained

<sup>1</sup><http://www.ahn.nl/>



through the rasterization of point clouds from AHN3 (2011-2019), while the aerial images<sup>2</sup> with the close date to AHN4 (2020-2022) are used as late period. The annotation procedure is as follows:

1) **Change definition.** The construction and demolition of buildings are annotated based on the difference map between AHN3 and AHN4. Since the capture date of aerial images does not precisely align with that of the point cloud, we have focused our annotations on multi-class building changes that remain relatively stable within a one-year time-frame, while excluding highly dynamic changes such as those involving trees and vehicles. Note that the demolished and newly-built buildings do not highly correspond to the negative and positive height change values due to tree occlusions and the penetration of low-reflectivity surfaces such as glass roofs, as depicted in Figure 4. We define a mask that indicates whether the building changes are highly relevant to their height change values, which is

$$M(i, j) = \begin{cases} 1, & \text{highly relevant} \\ -1, & \text{otherwise} \end{cases} \quad (7)$$

2) **Edge situation.** The second row of column (f) in Figure 6 shows a sophisticated situation where multiple building changes overlap with each other. This implies a sequence of events where a building is first demolished and subsequently replaced with a new one. For such a situation, the change type is determined based on the elevation difference, where pixels with a positive change in height are categorized as newly built, while pixels with a negative change in height are associated with demolished building changes. While we

---

<sup>2</sup><https://www.beeldmateriaal.nl/over-beeldmateriaal>

have provided a simplified representation by aggregating these overlapping changes into single-type changes, there remains an opportunity for future research to delve into finer sub-situations, describing the entire evolution process.

3) **Change label generation.** Based on the above-mentioned change definition and edge situation, the change map (CM) is formulated as

$$CM(i, j) = \begin{cases} \text{demolished, } \Delta H \cdot M(i, j) < 0 \text{ and building in early period} \\ \text{newly-built, } \Delta H \cdot M(i, j) > 0 \text{ and building in late period} \\ \text{background, } otherwise. \end{cases} \quad (8)$$

where  $\Delta H$  is the elevation difference between the bi-temporal DSM data, i.e.,  $\Delta H = DSM_{AHN4} - DSM_{AHN3}$ . The definition of the first two cases implies a sub-situation of bi-temporal buildings. The 2D change labels are generated according to the building boundaries in the DSM data, where they are strictly orthographic. It may be a little misaligned with the building in image data due to viewpoint distortion. The labels for 3D height changes correspond to the masked regions in the AHN4-to-AHN3 difference map.

4) **Tile splitting.** The original tile size of each city is  $25000 \times 20000$  with a pixel granularity of 0.25 meter, which is subsequently split into 500 pairs of  $1000 \times 1000$  sized samples. Note that we retained samples that do not include changes to better reflect the data distribution of the real-world scenario.

**Challenges of Hi-BCD dataset.** The fundamental challenge of our dataset is to learn the representation of multi-class elevation changes from multimodal and cross-dimensional inputs. There are some inherent misalignment between the multimodal inputs. 1) The pixels hold diverse implications

as the DSMs rasterize the height dimension from Lidar point clouds and represent the absolute land elevation, while the images reflect the intensity of visible light. They have vastly different numerical ranges, where the height range is  $[-8.24, 183.64]$  for original DSM and  $[-99.55, 134.21]$  for the changes in the training set, while the image values are in grayscale  $[0, 255]$ . 2) Their distribution differs a lot as the DSMs exhibit similar height in the ground regions, while the images portray different colors and textures for various land cover. 3) There exist geometry misalignment due to viewpoint distortion of aerial images although they utilize the same coordinate system. Furthermore, severe change-unchange imbalance can be observed. Additionally, there is inconsistency between the semantic change labels and the height change labels as shown in Figure 4.

## 5. Experiments and Results

### 5.1. Experiment setting

**Implementation details.** The tanh function is used to normalize height outputs to  $[-1, 1]$ . The elevation scale of training set  $[-27.29, 87.26]$  covering 99.5% of pixels is used for denormalization. We set class weights of 0.05, 0.95 and 0.95 to the background, demolished, and newly-built areas for weighted cross-entropy loss. All the models are pre-trained in LEVIR-CD [45] and then trained for 300 epochs with equivalent batch size 8. At ease of multi-scale downsampling, the original tile size of  $1000 \times 1000$  is adjusted to  $1024 \times 1024$  during training. More details can be found here<sup>3</sup>.

---

<sup>3</sup><https://github.com/qaz670756/MMCD>

**Metrics.** For semantic change detection evaluation, we used the mean intersection over union (mIoU) and F1-score as denoted in [18]. For the height change detection, we keep consistent with relevant research [18, 46, 47], including the following metrics:

- Root Mean Square Error (RMSE):  $\sqrt{\frac{1}{n} \sum (H_r - H_e)^2}$
- Mean Average Error (MAE):  $\frac{1}{n} \sum |H_r - H_e|$
- Root Mean Square Error (cRMSE):  $\sqrt{\frac{1}{n} \sum (H_r - H_e)^2}$
- Average relative error (cRel):  $\frac{1}{n} \sum \frac{|H_r - H_e|}{H_r}$
- Mean normalized cross correlation (ZNCC):  $\frac{1}{N} \sum_i \frac{(H_{ri} - \mu_{H_r})(H_{ei} - \mu_{H_e})}{\sigma_{H_r} \sigma_{H_e}}$

where  $H_r$  denotes the reference height,  $H_e$  denotes the estimated height, and  $N$  denotes the estimated pixel count.  $\mu$  and  $\sigma$  are the mean values and standard deviations of  $H_r$  and  $H_e$ , respectively. The cRMSE and cRel means that only changed areas are considered. The ZNCC quantifies the spatial correlation between output and ground truth, while the other metrics measure the degree of absolute errors at each pixel in meters. Moreover, we involve the million parameter amount (MParams) and Giga Floating-Point Operations (GFLOPs) to compare the model complexity [9, 48].

**Compared methods.** There is actually limited research [18] that detects semantic and height change concurrently. To provide a benchmarking, we follow the structure of MTBIT [18] that maintains the original change detection network while slightly modifying the decoder with an additional height change detection branch. Among the selected methods, the **FC-Siamese** [21] is the first fully convolution-based change detection architecture that is widely used for comparison. The **SNUNet** [19] is a state-of-the-

art CNN-based method with densely connected backbone. The **ChangeFormer** [43] is a Transformer-based method that yields promising results in current change detection benchmarks. The **P2VNet** [23] models the change process in a novel multi-frame transition perspective. The **MTBIT** is the latest Transformer-based network derived from BIT [9] to detect semantic and height changes simultaneously.

### 5.2. Comparison with state-of-the-arts

Table 3: The semantic change detection performance before and after attaching the height predicting branch. The methods with \* are originally designed with a height branch. The colors red, green and blue indicate the top three.

Method	Year	only semantic cd branch				semantic + height cd branch				Complexity (two branches)	
		$IoU_D \uparrow$	$IoU_N \uparrow$	mIoU $\uparrow$	F1-score $\uparrow$	$IoU_D \uparrow$	$IoU_N \uparrow$	mIoU $\uparrow$	F1-score $\uparrow$	MParams $\downarrow$	GFLOPs $\downarrow$
FC-Siamese [21]	2018	27.77	29.18	28.48	44.33	27.60	28.34	27.97	43.72	1.552	92.908
SNUNet [19]	2021	25.47	26.07	25.77	40.98	20.77	22.97	21.87	35.87	3.012	220.696
ChangeFormer [43]	2022	47.17	36.67	41.92	58.88	38.89	41.45	40.17	57.31	29.75	340.165
P2VNet [23]	2022	37.41	30.61	34.00	50.65	35.63	30.46	33.04	49.62	5.425	527.442
*MTBIT [18]	2023	37.44	29.97	33.71	50.31	34.40	27.04	30.72	46.88	15.2	154.72
*Ours	2023	43.76	39.10	41.43	58.55	44.29	40.90	42.59	59.72	11.659	168.893

In this section, we conduct an evaluation of semantic and height change detection to explore how these two tasks influence each other. Note that semantic change detection refers to multi-class 2D change detection in our context. The model operates in a multitask situation when performing joint semantic and height change detection. Otherwise, it is in a single-task setting.

**Semantic change detection.** As shown in Table 3, our method achieves competitive semantic results in both single-task and multitask settings. Specifically, by employing a single semantic change detection branch, we achieve close results to ChangeFormer with only half the model complexity. Besides

that, the model with the largest number of parameters (ChangeFormer) and highest computational cost (P2VNet) achieved the second and third best places. When augmented with our consistency-enhanced height prediction branch, the metric numbers exhibit continued improvement. On the contrary, the other methods that attached to the height change detection branch without consistency constraint, show a notable degradation. It implies that the added height change detection branch hinders the learning of semantic branch, where a similar phenomenon is also observed in prior works [49, 50]. Different optimization objectives among multiple tasks can lead to potential mutual interference during feature optimization. With the help of the consistency constraint, our method prevents performance degradation due to interference from the height change detection branch.

Table 4: The height change detection performance without and with semantic branch. The underlined numbers indicate a decrease with the attached semantic change detection branch compared to its single-branch counterpart. The methods with \* are originally designed with a height branch. The colors **red**, **green** and **blue** indicate the top three.

Method	only height cd branch					semantic + height cd branch				
	RMSE↓	MAE↓	cRMSE↓	cRel↓	cZNCC↑	RMSE↓	MAE↓	cRMSE↓	cRel↓	cZNCC↑
FC-Siamese	<b>1.505</b>	0.446	<b>8.622</b>	<b>1.838</b>	<b>0.274</b>	1.461	<b>0.309</b>	<u>8.995</u>	<b>1.506</b>	0.373
SNUNet	1.574	0.498	9.397	2.988	0.186	<u>1.671</u>	<u>0.779</u>	9.216	2.704	0.265
ChangeFormer	1.658	<b>0.313</b>	<b>8.404</b>	2.110	<b>0.308</b>	<b>1.343</b>	<u>0.402</u>	<b>8.204</b>	<u>2.485</u>	<b>0.394</b>
P2V-CD	<b>1.392</b>	<b>0.399</b>	9.037	<b>1.937</b>	0.261	<u>1.408</u>	<b>0.305</b>	8.932	<b>1.463</b>	<b>0.377</b>
*MTBIT	1.530	0.475	9.441	<b>1.780</b>	0.179	1.457	0.400	<b>8.563</b>	<u>1.987</u>	0.345
*Ours	<b>1.273</b>	<b>0.397</b>	<b>8.317</b>	2.711	<b>0.379</b>	<b>1.267</b>	<b>0.290</b>	<b>8.281</b>	<b>1.900</b>	<b>0.394</b>

**Height change detection.** In Table 4, it is interesting that among the 30 metric results obtained with a height change detection branch, 23 of them gain improvements when working with a semantic branch, while only

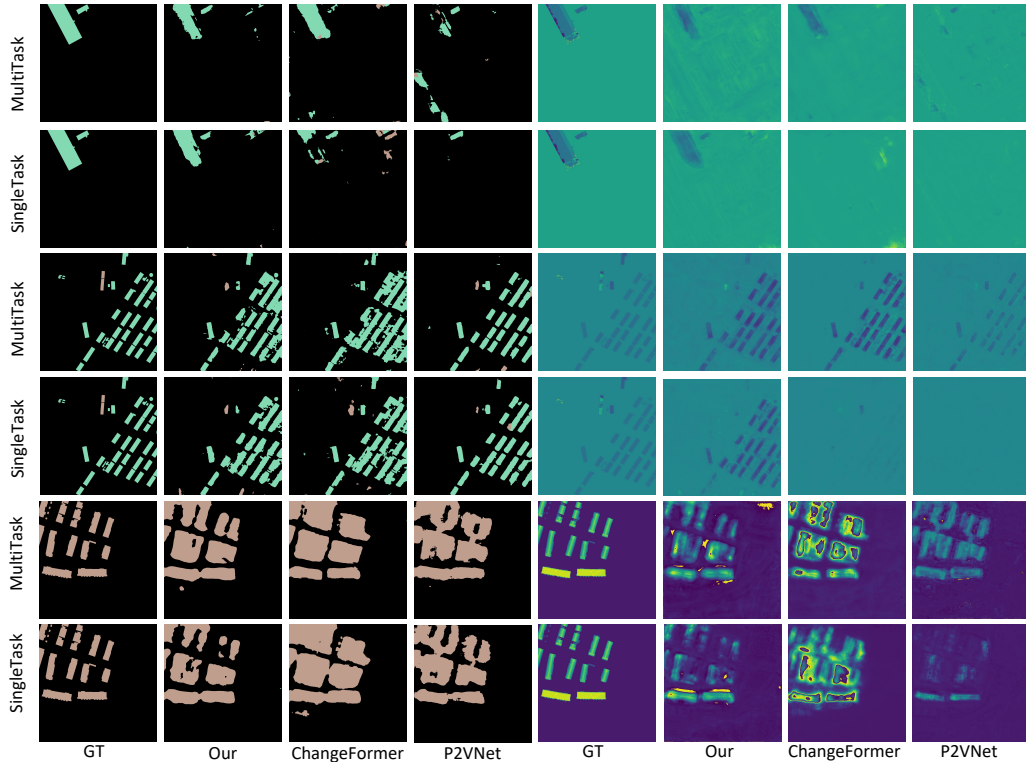


Figure 8: Visual comparison of semantic (first four columns) and height (last four columns) for the top-three methods in single-task (only semantic or height branch) and multitask change detection scenarios. Note that the single-task height change detection results are from the consistency augmented height branch corresponding to in row 3 of Table 5.

7 of them show a decrease. This phenomenon clearly highlights the positive impact of learning the shared representation through the implicit hints from semantic change. As also denoted in [49], the object boundaries are easier to capture from the semantic map compared to the depth map. By incorporating an additional branch dedicated to predicting pseudo changes based on the height map, we establish an explicit correlation between semantic and height changes. This enhancement is evident in the improved performance

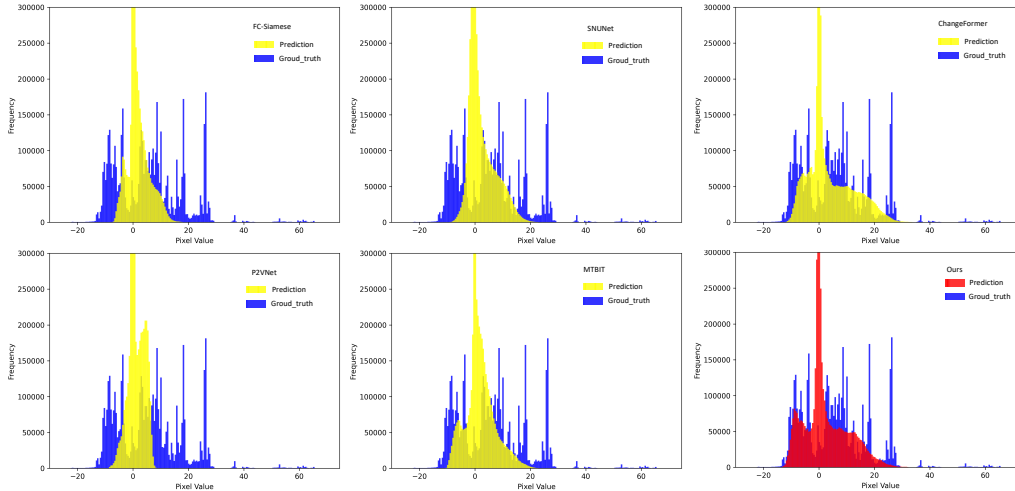


Figure 9: The comparison of predicted height distribution, where blue denotes ground truth, yellow and red denote the other methods and ours.

of height change detection across five different metrics.

**Qualitative Results.** Figure 8 depicts the visual comparison of semantic and height change detection for the top three methods. The tendency could be observed in the first four columns of Figure 8. From the last four columns, we could observe collapsed results from those models without semantic hints in single-task setting, except for ours. Note that the single-task visual results of our method are derived from the height change detection branch that is augmented with multitask consistency.

Figure 9 provides a height prediction comparison in a distribution manner. For the value range of height change, the other change detection methods tend to underestimate, while our method outputs a more precise range. For the distribution of output height, most methods output a single peak near zero except for ChangeFormer, MTBIT, and our method, while the real dis-



tribution has at least two major clustered regions. However, We observe that the dominant portion of height outputs for all methods is near zero. This reflects the influence of background to changed areas imbalance. We remain this problem as a future direction.

### 5.3. Ablation study

In this section, we explore the influences of the proposed multitask consistency for semantic and height change detection. Initially, We demonstrate that the implicit information shared at the backbone stage yields benefits for height change detection while concurrently posing challenges for semantic change detection.

From the results of row 1 and row 3 in Table 5, an evident decline in semantic change detection can be observed. On the contrary, the height metric results from row 2 and row 3 indicate that the semantic hint is beneficial for estimating the height changes, even with only implicit shared information in the common backbone. Figure 10(b)(c)(e)(f) illustrates some visual examples wherein the semantic branch exhibits improved recovery of height changes.

Table 5: Ablation study about the impact of multitask consistency (+MC) on height change predicting branch (+3d) and semantic change detection (+2d) in single-task or multitask scenarios.

Settings			Semantic metrics				Height metrics				
+2d	+3d	+MC	$IoU_D$	$IoU_N$	mIoU	F1score	RMSE	MAE	CRMSE	cRel	ZNCC
✓			43.76	39.10	41.43	58.55	-	-	-	-	-
	✓		-	-	-	-	1.460	0.301	8.289	2.075	0.311
✓	✓		39.05	37.31	38.18	55.26	1.367	0.358	8.875	1.922	0.311
	✓	✓	-	-	-	-	1.273	0.397	8.317	2.711	0.379
✓	✓	✓	44.29	40.90	42.59	59.72	1.267	0.290	8.281	1.900	0.394

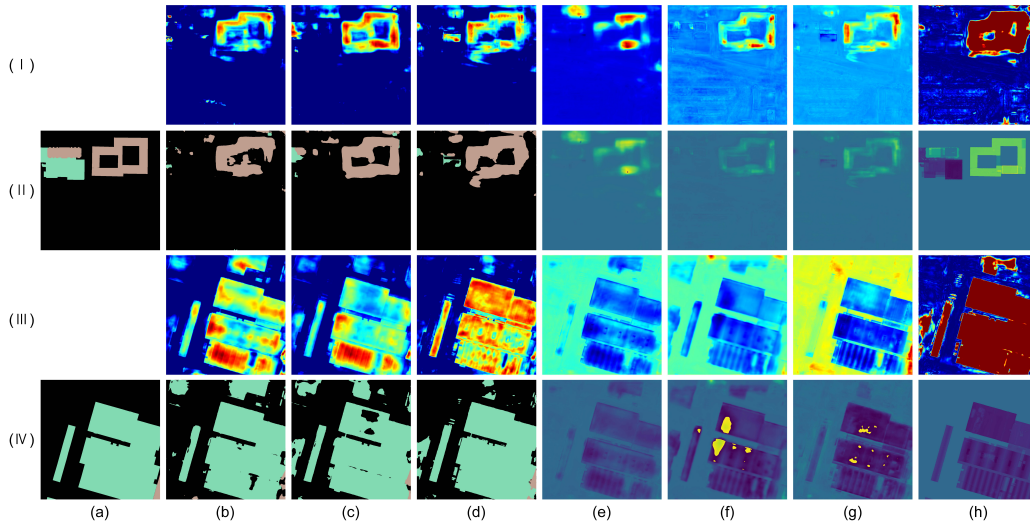


Figure 10: Visual examples highlighting the improvement via multitask interaction. (a) semantic ground truth; (b)(e) single-task results and corresponding attention maps; (c)(f) multitask results and corresponding attention maps; (d)(g) multitask results and corresponding attention maps with consistency constraint; (h) attention maps for soft thresholding layer (odd-numbered rows) and ground truth height changes (even-numbered rows).

However, it tends to introduce more noise in the background regions. From the odd-numbered rows of columns (c) and (f), we can observe that the attention regions corresponding to the semantic output closely resemble height changes. This suggests a strong coupling between their learned representations, which is the reason why the inclusion of the height branch poses challenges for semantic change detection, resulting in suboptimal performance in both tasks, as demonstrated in Figure 11(b)(c)(e)(f). To alleviate the problem, we designed the pseudo-change branch for two purposes:

1) When there is no hint from the semantic change branch available, it serves as a sub-complete semantic map to assist in the height change detection, resulting in an augmented height detection branch. Comparing row

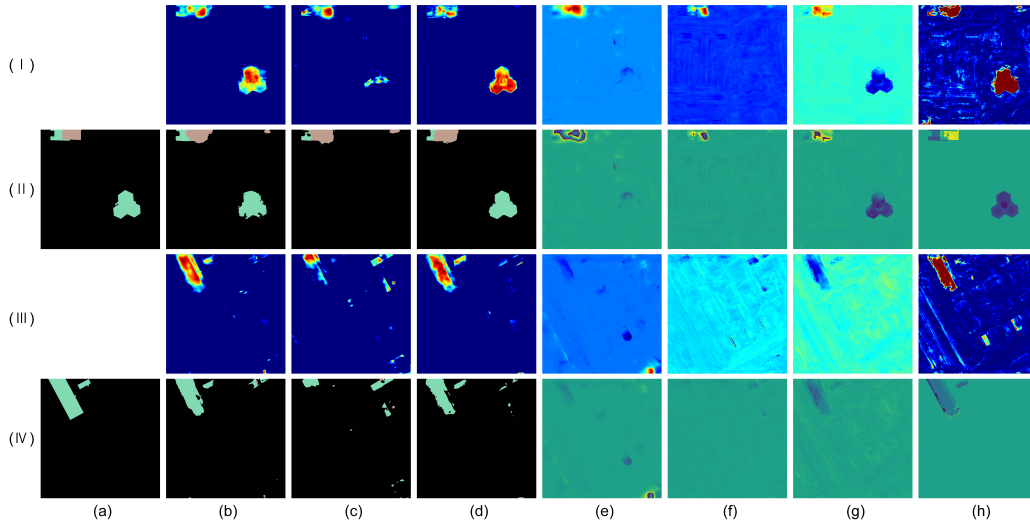


Figure 11: Visual examples highlighting the decline due to multitask branches. (a) semantic ground truth; (b)(e) single-task results and corresponding attention maps; (c)(f) multitask results and corresponding attention maps; (d)(g) multitask results and corresponding attention maps with consistency constraint; (h) attention maps for soft thresholding layer (odd-numbered rows) and ground truth height changes (even-numbered rows).

2 to row 4 in Table 5, we found that the semantic hint from the pseudo change branch is even better than the original semantic branch. We speculate that it was attributed to the explicit soft thresholding process, which brings stronger prior about multitask relationship than the limited hints from shared backbone. The odd-numbered rows of the final column in Figure 10 and 11 provide a visualization of learned representation in the soft thresholding layer, which accurately locates some edge cases that were missed by the original multitask scenario.

2) When there are semantic and height change branches exist, the pseudo change branch plays the role of building a consistent relationship between the two tasks. Interestingly, the final row of Table 5 demonstrates that

Table 6: The impact of our consistency strategy on the other methods, including one CNN-based and two Transformer-based change detection models. The **bold** font indicates better results.

Settings	Heightmetrics					Semanticmetrics	
	RMSE	MAE	cRMSE	cRel	ZNCC	mIoU $\uparrow$	F1-score $\uparrow$
FC-siamese	1.461	<b>0.309</b>	8.995	<b>1.506</b>	0.373	27.97	43.72
+multitask consistency	<b>1.398</b>	0.353	<b>8.655</b>	1.873	<b>0.395</b>	<b>28.85</b>	<b>44.78</b>
ChangeFormer	1.343	0.402	8.204	2.485	0.394	40.17	57.31
+multitask consistency	<b>1.317</b>	<b>0.297</b>	<b>8.085</b>	<b>1.825</b>	<b>0.447</b>	<b>41.37</b>	<b>58.39</b>
MTBIT	1.457	0.400	<b>8.563</b>	1.987	<b>0.345</b>	30.72	46.88
+multitask consistency	<b>1.373</b>	<b>0.343</b>	8.788	<b>1.639</b>	0.281	<b>32.44</b>	<b>48.90</b>

our consistency strategy has not only mitigated the multitask conflicts, but also encouraged further improvements via explicit multitask interaction, as shown in Figure 10(d)(g) and 11(d)(g). Furthermore, our consistency strategy can be seamlessly applied to the other change detection methods and yields promising improvements, as shown in Table 6.

To further investigate the impact of our consistency constraint on height change detection, We varied the temperature parameter of equation 4. Figure 12 shows that a smaller temperature value leads to a sharper transition near zero and greater overlap between the ground truth and predicted height change. This is because the sharp transition near zero suppresses background

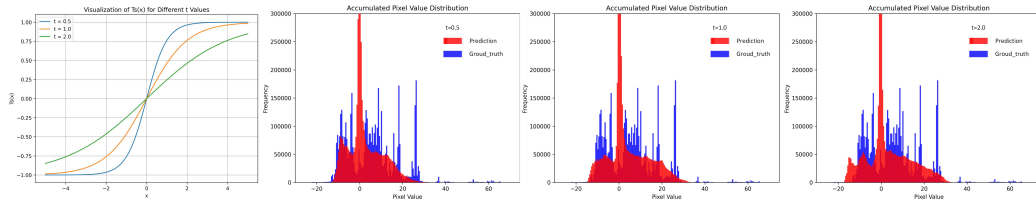


Figure 12: The impact of different  $t$  values on height change detection.

noise where height is unchanged, allowing more attention on changed regions. However, this parameter is a double-edged sword; a too-small value means that background noise is more likely to be mistaken for a change target. Therefore, in our experiments, we set  $t$  to 0.5 as the final setting.

#### 5.4. Discussion

The experiment results strongly emphasize the multitask conflicts between 2D semantic change detection and 3D height estimation. Specifically, the semantic change exhibits a distinct boundary that aids in pinpointing changes compared to height change estimation. A similar phenomenon has been documented in [49], which highlights that object boundaries are more readily discerned from segmentation labels than from depth maps. From Figure 10 and 11, we could observe the inherent consistency between height change and the activation map of semantic change within a single testing example. This suggests that the decreased performance of the multitask setting is mainly caused by the height branch. As denoted in [50], jointly addressing semantic segmentation and depth estimation tasks tends to yield suboptimal results compared to single-task settings.

Our proposed multitask consistency constraint has connected the height change branch and pseudo-change branch via soft-thresholding. By minimizing the disparity between pseudo-change and semantic change, we enable gradient interaction from the semantic change map to the height change map. This establishes a coherent objective for the multitask branches and ultimately enhances the performance of both tasks, as evidenced in our experiments.

## 6. Conclusion

The prevailing direction in change detection research is toward achieving higher frequency, finer granularity, and increased dimensionality. However, there exists a noticeable gap in the literature pertaining to multimodal and cross-dimensional change detection. In this paper, we presented a novel pipeline for detecting height and semantic change simultaneously from DSM-to-image multimodal data. We revealed that the leading change detection methods, including CNN-based and Transformer-based methods, struggled with the conflicts of multitask change detection. We proposed a Transformer-based network equipped with multitask consistency constraint, which achieves the best semantic and height change detection performance with limited model complexity. We found that the consistency strategy with a small temperature parameter is able to suppress the background noise and leads to sharper results in change regions. It can be also seamlessly employed to the other change detection methods and produce promising improvements.

## References

### References

- [1] A. Toker, L. Kondmann, M. Weber, M. Eisenberger, A. Camero, J. Hu, A. P. Hoderlein, Ç. Şenaras, T. Davis, D. Cremers, et al., Dynamicearthnet: Daily multi-spectral satellite dataset for semantic change segmentation, in: Proceedings of the IEEE/CVF Conference on Computer Vision and Pattern Recognition, 2022, pp. 21158–21167.
- [2] S. Tian, Y. Zhong, Z. Zheng, A. Ma, X. Tan, L. Zhang, Large-scale deep learning based binary and semantic change detection in ultra high

- resolution remote sensing imagery: From benchmark datasets to urban application, *ISPRS Journal of Photogrammetry and Remote Sensing* 193 (2022) 164–186.
- [3] M. Cserép, R. Lindenbergh, Distributed processing of dutch ahn laser altimetry changes of the built-up area, *International Journal of Applied Earth Observation and Geoinformation* 116 (2023) 103174.
- [4] U. Stilla, Y. Xu, Change detection of urban objects using 3d point clouds: A review, *ISPRS Journal of Photogrammetry and Remote Sensing* 197 (2023) 228–255.
- [5] Y. Zhan, K. Fu, M. Yan, X. Sun, H. Wang, X. Qiu, Change detection based on deep siamese convolutional network for optical aerial images, *IEEE Geoscience and Remote Sensing Letters* 14 (10) (2017) 1845–1849. doi:10.1109/LGRS.2017.2738149.
- [6] S. Zagoruyko, N. Komodakis, Learning to compare image patches via convolutional neural networks, in: *Proceedings of the IEEE conference on computer vision and pattern recognition*, 2015, pp. 4353–4361.
- [7] Y. Quan, A. Yu, W. Guo, X. Lu, B. Jiang, S. Zheng, P. He, Unified building change detection pre-training method with masked semantic annotations, *International Journal of Applied Earth Observation and Geoinformation* 120 (2023) 103346.
- [8] D. Peng, L. Bruzzone, Y. Zhang, H. Guan, H. Ding, X. Huang, Semicd-net: A semisupervised convolutional neural network for change detec-

- tion in high resolution remote-sensing images, *IEEE Transactions on Geoscience and Remote Sensing* 59 (7) (2020) 5891–5906.
- [9] H. Chen, Z. Qi, Z. Shi, Remote sensing image change detection with transformers, *IEEE Transactions on Geoscience and Remote Sensing* 60 (2021) 1–14.
- [10] C. Zhang, L. Wang, S. Cheng, Y. Li, Swinsunet: Pure transformer network for remote sensing image change detection, *IEEE Transactions on Geoscience and Remote Sensing* 60 (2022) 1–13.
- [11] R. Touati, M. Mignotte, An energy-based model encoding nonlocal pairwise pixel interactions for multisensor change detection, *IEEE Transactions on Geoscience and Remote Sensing* 56 (2) (2017) 1046–1058.
- [12] H. Chen, N. Yokoya, C. Wu, B. Du, Unsupervised multimodal change detection based on structural relationship graph representation learning, *IEEE Transactions on Geoscience and Remote Sensing* 60 (2022) 1–18.
- [13] Z. Zhang, G. Vosselman, M. Gerke, C. Persello, D. Tuia, M. Yang, Change detection between digital surface models from airborne laser scanning and dense image matching using convolutional neural networks, *ISPRS Annals of the Photogrammetry, Remote Sensing and Spatial Information Sciences* 4 (2019) 453–460.
- [14] R. Touati, M. Mignotte, M. Dahmane, Multimodal change detection in remote sensing images using an unsupervised pixel pairwise-based markov random field model, *IEEE Transactions on Image Processing* 29 (2019) 757–767.



- [15] G. Fodor, M. V. Conde, Rapid deforestation and burned area detection using deep multimodal learning on satellite imagery, arXiv preprint arXiv:2307.04916 (2023).
- [16] Z. Zhang, Photogrammetric point clouds: quality assessment, filtering, and change detection (2022).
- [17] H. Zhang, M. Wang, F. Wang, G. Yang, Y. Zhang, J. Jia, S. Wang, A novel squeeze-and-excitation w-net for 2d and 3d building change detection with multi-source and multi-feature remote sensing data, *Remote Sensing* 13 (3) (2021) 440.
- [18] V. Marsocci, V. Coletta, R. Ravanelli, S. Scardapane, M. Crespi, Inferring 3d change detection from bitemporal optical images, *ISPRS Journal of Photogrammetry and Remote Sensing* 196 (2023) 325–339.
- [19] S. Fang, K. Li, J. Shao, Z. Li, Snunet-cd: A densely connected siamese network for change detection of vhr images, *IEEE Geoscience and Remote Sensing Letters* 19 (2021) 1–5.
- [20] C. Zhang, P. Yue, D. Tapete, L. Jiang, B. Shangguan, L. Huang, G. Liu, A deeply supervised image fusion network for change detection in high resolution bi-temporal remote sensing images, *ISPRS Journal of Photogrammetry and Remote Sensing* 166 (2020) 183–200.
- [21] R. C. Daudt, B. Le Saux, A. Boulch, Fully convolutional siamese networks for change detection, in: 2018 25th IEEE International Conference on Image Processing (ICIP), IEEE, 2018, pp. 4063–4067.

- [22] B. Liu, H. Chen, Z. Wang, Lsnet: Extremely light-weight siamese network for change detection in remote sensing image, arXiv preprint arXiv:2201.09156 (2022).
- [23] M. Lin, G. Yang, H. Zhang, Transition is a process: Pair-to-video change detection networks for very high resolution remote sensing images, *IEEE Transactions on Image Processing* 32 (2022) 57–71.
- [24] D. Peng, L. Bruzzone, Y. Zhang, H. Guan, P. He, Scdnet: A novel convolutional network for semantic change detection in high resolution optical remote sensing imagery, *International Journal of Applied Earth Observation and Geoinformation* 103 (2021) 102465.
- [25] R. Qin, J. Tian, P. Reinartz, 3d change detection—approaches and applications, *ISPRS Journal of Photogrammetry and Remote Sensing* 122 (2016) 41–56.
- [26] I. de Gélis, S. Saha, M. Shahzad, T. Corpetti, S. Lefèvre, X. X. Zhu, Deep unsupervised learning for 3d als point clouds change detection, arXiv preprint arXiv:2305.03529 (2023).
- [27] V. Ferraris, N. Dobigeon, Y. Cavalcanti, T. Oberlin, M. Chabert, Coupled dictionary learning for unsupervised change detection between multimodal remote sensing images, *Computer Vision and Image Understanding* 189 (2019) 102817.
- [28] S. Chirakkal, F. Bovolo, A. Misra, L. Bruzzone, A. Bhattacharya, Unsupervised multiclass change detection for multimodal remote sensing

- data, in: IGARSS 2022-2022 IEEE International Geoscience and Remote Sensing Symposium, IEEE, 2022, pp. 3223–3226.
- [29] Y. Sun, L. Lei, X. Tan, D. Guan, J. Wu, G. Kuang, Structured graph based image regression for unsupervised multimodal change detection, *ISPRS Journal of Photogrammetry and Remote Sensing* 185 (2022) 16–31.
- [30] L. T. Luppino, M. Kampffmeyer, F. M. Bianchi, G. Moser, S. B. Serpico, R. Jenssen, S. N. Anfinsen, Deep image translation with an affinity-based change prior for unsupervised multimodal change detection, *IEEE Transactions on Geoscience and Remote Sensing* 60 (2021) 1–22.
- [31] X. Li, Z. Du, Y. Huang, Z. Tan, A deep translation (gan) based change detection network for optical and sar remote sensing images, *ISPRS Journal of Photogrammetry and Remote Sensing* 179 (2021) 14–34.
- [32] Y. Wu, J. Li, Y. Yuan, A. Qin, Q.-G. Miao, M.-G. Gong, Commonality autoencoder: Learning common features for change detection from heterogeneous images, *IEEE transactions on neural networks and learning systems* 33 (9) (2021) 4257–4270.
- [33] R. Shao, C. Du, H. Chen, J. Li, Sunet: Change detection for heterogeneous remote sensing images from satellite and uav using a dual-channel fully convolution network, *Remote Sensing* 13 (18) (2021) 3750.
- [34] M. Yang, L. Jiao, F. Liu, B. Hou, S. Yang, M. Jian, Dpfl-nets: Deep pyramid feature learning networks for multiscale change detection, *IEEE*

- Transactions on Neural Networks and Learning Systems 33 (11) (2021) 6402–6416.
- [35] Z. Zhang, G. Vosselman, M. Gerke, D. Tuia, M. Y. Yang, Change detection between multimodal remote sensing data using siamese cnn, arXiv preprint arXiv:1807.09562 (2018).
- [36] C.-F. R. Chen, Q. Fan, R. Panda, Crossvit: Cross-attention multi-scale vision transformer for image classification, in: Proceedings of the IEEE/CVF international conference on computer vision, 2021, pp. 357–366.
- [37] Z. Zheng, Y. Zhong, S. Tian, A. Ma, L. Zhang, Changemask: Deep multi-task encoder-transformer-decoder architecture for semantic change detection, ISPRS Journal of Photogrammetry and Remote Sensing 183 (2022) 228–239.
- [38] K. Yang, G.-S. Xia, Z. Liu, B. Du, W. Yang, M. Pelillo, L. Zhang, Asymmetric siamese networks for semantic change detection in aerial images, IEEE Transactions on Geoscience and Remote Sensing 60 (2021) 1–18.
- [39] Y. Deng, J. Chen, S. Yi, A. Yue, Y. Meng, J. Chen, Y. Zhang, Feature-guided multitask change detection network, IEEE Journal of Selected Topics in Applied Earth Observations and Remote Sensing 15 (2022) 9667–9679.
- [40] R. C. Daudt, B. Le Saux, A. Boulch, Y. Gousseau, Multitask learning

- for large-scale semantic change detection, *Computer Vision and Image Understanding* 187 (2019) 102783.
- [41] Q. Shu, J. Pan, Z. Zhang, M. Wang, Mtcnet: Multitask consistency network with single temporal supervision for semi-supervised building change detection, *International Journal of Applied Earth Observation and Geoinformation* 115 (2022) 103110.
- [42] W. Wang, E. Xie, X. Li, D.-P. Fan, K. Song, D. Liang, T. Lu, P. Luo, L. Shao, Pyramid vision transformer: A versatile backbone for dense prediction without convolutions, in: *Proceedings of the IEEE/CVF international conference on computer vision*, 2021, pp. 568–578.
- [43] W. G. C. Bandara, V. M. Patel, A transformer-based siamese network for change detection, in: *IGARSS 2022-2022 IEEE International Geoscience and Remote Sensing Symposium*, IEEE, 2022, pp. 207–210.
- [44] K. He, X. Zhang, S. Ren, J. Sun, Deep residual learning for image recognition, in: *Proceedings of the IEEE conference on computer vision and pattern recognition*, 2016, pp. 770–778.
- [45] H. Chen, Z. Shi, A spatial-temporal attention-based method and a new dataset for remote sensing image change detection, *Remote Sensing* 12 (10) (2020) 1662.
- [46] W. Zhao, C. Persello, A. Stein, Semantic-aware unsupervised domain adaptation for height estimation from single-view aerial images, *ISPRS Journal of Photogrammetry and Remote Sensing* 196 (2023) 372–385.

- [47] H. A. Amirkolaee, H. Arefi, Height estimation from single aerial images using a deep convolutional encoder-decoder network, *ISPRS journal of photogrammetry and remote sensing* 149 (2019) 50–66.
- [48] B.-Y. Liu, H.-X. Chen, Z. Huang, X. Liu, Y.-Z. Yang, Zoominnet: A novel small object detector in drone images with cross-scale knowledge distillation, *Remote Sensing* 13 (6) (2021) 1198.
- [49] S. Zhu, G. Brazil, X. Liu, The edge of depth: Explicit constraints between segmentation and depth, in: *Proceedings of the IEEE/CVF conference on computer vision and pattern recognition*, 2020, pp. 13116–13125.
- [50] B. Liu, X. Liu, X. Jin, P. Stone, Q. Liu, Conflict-averse gradient descent for multi-task learning, *Advances in Neural Information Processing Systems* 34 (2021) 18878–18890.